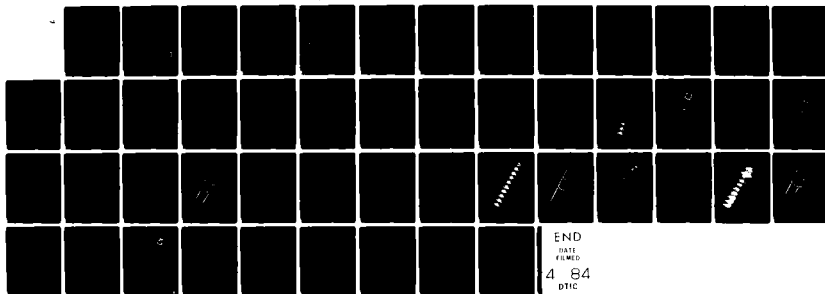AD-A138 649   THREE-DIMENSIONAL TWO-PHASE SUPERSONIC NOZZLE FLOWS(U)   1/1
               AEROSPACE CORP EL SEGUNDO CA VEHICLE ENGINEERING DIV
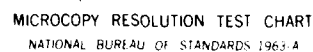   I S CHANG 01 OCT 83 TR-0084(9975)-2 F04701-83-C-0084

UNCLASSIFIED   F/G 20/4   NL

END
DATE
FILMED
4 84
DTIC

MICROCOPY RESOLUTION TEST CHART

NATIONAL BUREAU OF STANDARDS 1963-A

⑫

AD A138649

Three-Dimensional, Two-Phase Supersonic Nozzle Flows

I-S. CHANG
Vehicle Engineering Division
Engineering Group
The Aerospace Corporation
El Segundo, Calif. 90245

1 October 1983

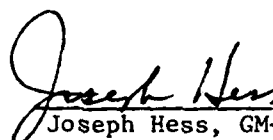Final Report

DTIC
SELECTED
MAR 0 8 1984
E

DTIC FILE COPY

84 03 06 054

This final report was submitted by The Aerospace Corporation, El Segundo, CA 90245, under Contract No. F04701-83-C-0084 with the Space Division, Deputy for Technology, P.O. Box 92960, Worldway Postal Center, Los Angeles, CA 90009. It was reviewed and approved for The Aerospace Corporation by E. G. Hertler, Principal Director, Aero Engineering Subdivision. 1st Lt D.A. Eyres was the project officer for Air Force.

This report has been reviewed by the Public Affairs Office (PAS) and is releasable to the National Technical Information Service (NTIS). AT NTIS, it will be available to the general public, including foreign nations.

This technical report has been reviewed and is approved for publication. Publication of this report does not constitute Air Force approval of the report's findings or conclusions. It is published only for the exchange and stimulation of ideas.

Dean A. Eyres, 1st Lt, USAF
Project Officer

Joseph Hess, GM-15, Director
West Coast Office, Air Force
Space Technology Center

REPORT DOCUMENTATION PAGE		READ INSTRUCTIONS BEFORE COMPLETING FORM
1. REPORT NUMBER SD-TR-83-91	2. GOVT ACCESSION NO. A138 649	3. RECIPIENT'S CATALOG NUMBER
4. TITLE (and Subtitle) THREE-DIMENSIONAL, TWO-PHASE SUPERSONIC NOZZLE FLOWS		5. TYPE OF REPORT & PERIOD COVERED Final Report Oct. 1980-Jan. 1982
		6. PERFORMING ORG. REPORT NUMBER TR-0084(9975)-2
7. AUTHOR(s) I-S. Chang		8. CONTRACT OR GRANT NUMBER(s) F04701-83-C-0084
9. PERFORMING ORGANIZATION NAME AND ADDRESS The Aerospace Corporation El Segundo, CA 90245		10. PROGRAM ELEMENT, PROJECT, TASK AREA & WORK UNIT NUMBERS
11. CONTROLLING OFFICE NAME AND ADDRESS		12. REPORT DATE 1 October 1983
		13. NUMBER OF PAGES 46
14. MONITORING AGENCY NAME & ADDRESS(If different from Controlling Office) Space Division, Air Force Systems Command Los Angeles Air Force Station P.O. Box 92960, Worldway Postal Center Los Angeles, CA 90009		15. SECURITY CLASS. (of this report) Unclassified
		15a. DECLASSIFICATION/DOWNGRADING SCHEDULE

16. DISTRIBUTION STATEMENT (of this Report)

Approved for public release; distribution unlimited.

17. DISTRIBUTION STATEMENT (of the abstract entered in Block 20, if different from Report)

18. SUPPLEMENTARY NOTES

19. KEY WORDS (Continue on reverse side if necessary and identify by block number)

Supersonic flows
Nozzle flows
Multi-phase flows

20. ABSTRACT (Continue on reverse side if necessary and identify by block number) Fully coupled two-phase supersonic flows inside three-dimensional nozzles of various configurations are studied, and the behavior of flows with and without solid particles is compared and discussed. The presence of solid particles in the supersonic flow delays gas-phase expansion and alters the imbedded compressive gas-phase shock strength. The results from the present study for an axisymmetric nozzle are compared with those of the well-known SPP code. Isometric projection of three-dimensional contour plots is used for concise interpretation of the computed results for a Mach 3 inlet one- and two-phase flow under various operating conditions.

DD FORM 1473
(FACSIMILE)

PREFACE

CONTENTS

FIGURES

I. INTRODUCTION

Since the formulation of the governing equations and pioneering work by researchers on solid rocket nozzle flows in the 1960s (e.g., Refs. 1 and 2), the theoretical approach to gas-particle flows has received increasing attention by the workers in the propulsion industry who are involved with the development of solid rocket motors (SRMs). The knowledge gained from theoretical two-phase SRM flowfield studies will lead to better predictions of motor performance, range, and payload delivery, improvement of motor in-depth thermal-structural analysis, and reduction in motor design, development, and test risks and cost. A complete description of the SRM flow field necessitates the consideration of combustion chamber, igniter, throat, and exhaust exit cone internal fully coupled chemically reacting viscous two-phase flow solution, which is by no means an easy task. Only the analysis of flow under idealized conditions is possible at the present time. In the subsonic-transonic regime, Ref. 3 provides a solution method for a two-phase inviscid flow inside the chamber and nozzle of arbitrary configurations. For the supersonic nozzle and exit cone flow, the widely used computer program[4] in the industry utilizes the method of characteristics. There is nothing wrong with applying the method of characteristics to the two-phase supersonic flow study, except that the extension of the method to three-dimensional space is not straight-forward. The inability to resolve flowfields containing shock waves is another drawback of adopting the method of characteristics, since almost any disturbance in a supersonic stream will produce one or more shock waves. A finite difference approach has recently been applied to nozzle and exhaust plume flows including gas-particle interactions.[5]

All the works cited above have been restricted to the flow in one- or two-dimensional space. Confronted with asymmetric nozzle mechanizations, such as the canted Titan SRM, fluid-bearing thrust vector control (TVC) inertial upper stage (IUS) motor, and the flexible bearing TVC space shuttle SRM, the rocket nozzle designer often appears in an unfavorable position. Currently, there is no analytical tool available in this regard. The scarce data obtained from expensive test measurements is usually the only source of design

7

basis. It is, therefore, highly desirable to have the theoretical capability of analyzing a two-phase flow inside a three-dimensional nozzle.

In this report, the three-dimensional one-phase formulation of Ref. 6 is extended to include the momentum and energy transfer between gas and particle phases in supersonic nozzle flows. The condition of constant entropy on the boundary surface is inadequate for the two-phase flow, even in the region where a shock does not interact with the boundary. Moreover, the expansion and compression wave structures in a two-phase nozzle flow are observed to differ from those in a clean gas nozzle flow. The effect of different particle size and gas specific heat ratio on the overall two-phase flow behavior is investigated through the calculation of a Mach 3 inlet flow inside a rounded square three-dimensional supersonic nozzle. Additional two-phase flow solutions using similar inlet flow conditions for various nozzle configurations are also presented. Isometric projection of three-dimensional contour plots is used for concise interpretation of the computed results and for visualization of flow structures inside three-dimensional nozzles.

II. FORMULATION

Normalized by the gas-phase stagnation state corresponding to the condition at the inlet plane, the governing equations written in weak conservative form for a steady three-dimensional two-phase flow take the following form:

$$\frac{\partial \bar{E}}{\partial z} + \frac{\partial \bar{F}}{\partial r} + \frac{\partial \bar{G}}{\partial \theta} + \bar{H} = 0 \tag{1}$$

$$\bar{E} = \begin{bmatrix} \rho u \\ \tau p + \rho u^2 \\ \rho u v \\ \rho u w \\ [e + (\gamma-1)p]u \\ \rho_j u_j (N-1) \\ \rho_j u_j^2 (N-1) \\ \rho_j u_j v_j (N-1) \\ \rho_j u_j w_j (N-1) \\ h_j u_j (N-1) \end{bmatrix} ; \quad \bar{F} = \begin{bmatrix} \rho v \\ \rho u v \\ \tau p + \rho v^2 \\ \rho v w \\ [e + (\gamma-1)p]v \\ \rho_j v_j (N-1) \\ \rho_j u_j v_j (N-1) \\ \rho_j v_j^2 (N-1) \\ \rho_j v_j w_j (N-1) \\ h_j v_j (N-1) \end{bmatrix} ; \quad \bar{G} = \frac{1}{r^\delta} \begin{bmatrix} \rho w \\ \rho u w \\ \rho v w \\ \tau p + \rho w^2 \\ [e + (\gamma-1)p]w \\ \rho_j w_j (N-1) \\ \rho_j u_j w_j (N-1) \\ \rho_j v_j w_j (N-1) \\ \rho_j w_j^2 (N-1) \\ h_j w_j (N-1) \end{bmatrix}$$

$$\bar{H} = \frac{\delta}{r^\delta} \begin{bmatrix} \rho v \\ \rho u v \\ \rho(v^2 - w^2) \\ 2\rho v w \\ [e + (\gamma-1)p]v \\ \rho_j v_j \\ \rho_j u_j v_j \\ \rho_j (v_j^2 - w_j^2) \\ 2\rho_j v_j w_j \\ h_j v_j \end{bmatrix} + (N-1)\rho_j A_j \begin{bmatrix} 0 \\ (u-u_j) \\ (v-v_j) \\ (w-w_j) \\ B_j \\ 0 \\ -(u-u_j) \\ -(v-v_j) \\ -(w-w_j) \\ -B_j \end{bmatrix}$$

9

with friction term

$$A_j = \frac{9}{2} \frac{\bar{\mu}_g f_j}{\bar{m}_j \bar{r}_j^2} \frac{\vec{L}}{\bar{V}_{max1}} \tag{2}$$

and energy exchange term

$$B_j = 2\gamma \left[\vec{q}_j \cdot \Delta\vec{q}_j - g_c(T_j - T) - g_r \epsilon_e(T_j^4 - T^4)\right] \tag{3}$$

where

$$g_c = N_{uj}/6 f_j P_r, \qquad g_r = \bar{\sigma}\bar{r}_j \bar{T}_{t1}^3 \ 3 C_p \bar{\mu}_g f_j$$

$$\vec{q}_j \cdot \Delta\vec{q}_j = u_j(u-u_j) + v_j(v-v_j) + w_j(w-w_j)$$

$$T = \frac{P}{\rho}; \quad T_j = [h_j/\gamma\rho_j - (u_j^2 + v_j^2 + w_j^2)]/\omega$$

The momentum transfer parameter f_j is defined as

$$f_j = C_D/C_{D_{Stokes}} \tag{4}$$

where C_D is the particle drag coefficient given in Ref. 7 and $C_{D_{Stokes}} = 24/Re_j$.

The heat transfer parameter, particle Nusselt number, is taken as[8]

$$N_{uj} = 2 + 0.459 \ R_{ej}^{0.55} \ P_r^{0.33} \tag{5}$$

The particle Reynolds number is based on the relative speed

$$|\Delta q_j| = \sqrt{(u-u_j)^2 + (v-v_j)^2 + (w-w_j)^2}$$

and is defined as follows:

$$R_{ej} = \frac{2 \ |\Delta\bar{q}_j| \bar{r}_j \bar{\rho}}{\bar{\mu}_g} = 2 \ |\Delta q_j| \rho \frac{\bar{r}_j}{\bar{\mu}_g} \frac{1}{\tau} \frac{\bar{P}_{t1}}{\bar{V}_{max1}} \tag{6}$$

10

The gas viscosity is evaluated from

$$\bar{\mu}_g = \bar{\mu}_{t1} \; (\bar{T}/\bar{T}_{t1})^A \tag{7}$$

As shown in Fig. 1, the geometry of the three-dimensional nozzle cross-sectional profiles is assumed to have at least one plane of symmetry, and the nozzle wall radial coordinate is described by $r_w(\Theta, z)$. The transformation of the physical irregular region of interest into a portion of a unit circle with the clustering of grid points in the region of greatest slope change is carried out in the same fashion as that in the one-phase flow.[6] The transformation relationship is

$$z = z$$

$$\zeta = \left| \frac{2}{\pi} \tan^{-1}(k_1 \tan [(a + b\eta)])\pi + a_1 \right| \Big/ b_1$$

$$\xi = \Theta$$

where $\eta = r/r_w$ and constants k_1, a, b, a_1, and b_1 are parameters used for the grid clustering control such that for $0 < k_1 < 1$

$\quad$ $a = -1/2$, $b = 1/2$, $a_1 = 1$, $b_1 = 1$ grid points are
$\quad$ $\quad$ clustered near $\eta = 0$.

$\quad$ $a = 0$, $b = 1/2$, $a_1 = 0$, $b_1 = 1$ grid points are
$\quad$ $\quad$ clustered near $\eta = 1$.

$\quad$ $a = -1/2$, $b = 1$, $a_1 = 1$, $b_1 = 2$ grid points are
$\quad$ $\quad$ clustered near $\eta = 0$ and $\eta = 1$.

The cross-sectional region of computation for the cylindrical coordinates in Ref. 6 was restricted to 90°; whereas in this two-phase study, the computational region can be 90° or expanded to 180°. In the transformed
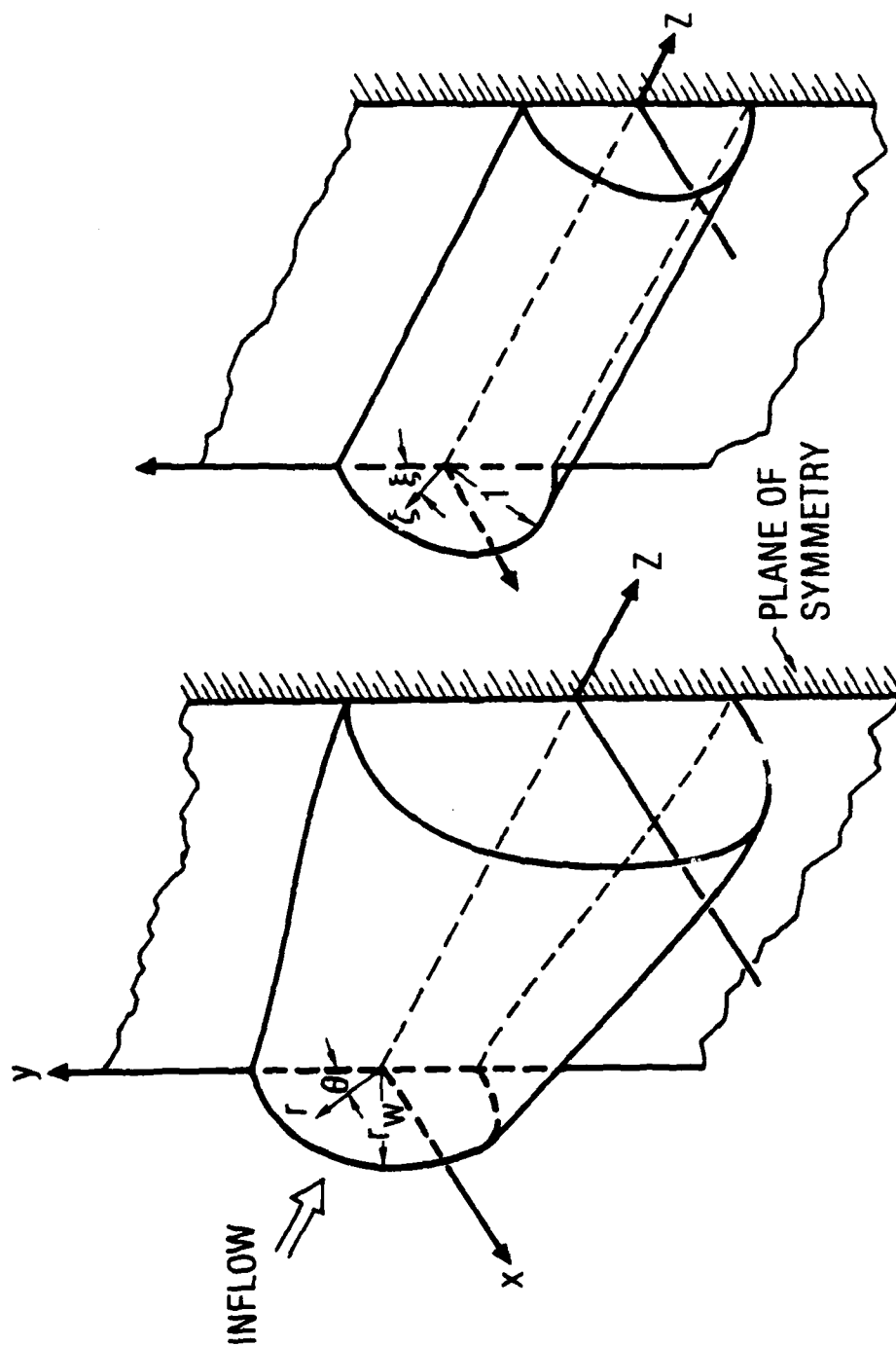
11

Fig. 1. Three-Dimensional Nozzle Coordinate System

space designated by a (z, ζ, ξ) coordinate system, the governing equations take the following form:

$$\frac{\partial E}{\partial z} + \frac{\partial F}{\partial \zeta} + \frac{\partial G}{\partial \xi} + H = 0 \tag{9}$$

where the vectors E, F, G, and H are related to $\tilde{E}$, $\tilde{F}$, $\tilde{G}$, and $\tilde{H}$ of Eq. (1) as follows:

$$E = \tilde{E}$$

$$F = \zeta_\eta \, [\tilde{F}\eta_r + \tilde{G}\eta_\theta + \tilde{E}\eta_z]$$

$$G = \tilde{G}$$

$$H = \tilde{H} - [\tilde{G}\eta_{\theta\eta} + \tilde{E}\eta_{z\eta}] - \zeta_{z\eta} \, [\tilde{F}\eta_r + \tilde{G}\eta_\theta + \tilde{E}\eta_z] \tag{10}$$

The subscripted variables indicate partial derivatives.[6]

III. SOLUTION METHOD

The weak conservative formulation, Eq. (5), is a hyperbolic type for supersonic flow along the main flow z direction and is solved by the MacCormack finite difference scheme.[9] The calculational procedure which utilizes the stability analysis described in Ref. 6 and a tangency condition for both gas and particle phase at the boundary surface are applied to the two-phase flow problem. Since two-phase flow is neither homentropic in the field nor isentropic at the boundary with or without the presence of shock interactions, the Abbett scheme[10] for determining gas phase boundary flow variables is modified to account for entropy change at the boundary. The flow variables obtained from the application of predictor and corrector steps[9] of the finite difference method, in general, will not satisfy the tangent flow condition on the nozzle surface in an inviscid analysis, and the Abbett scheme amounts to correcting the pressure through the use of a simple wave to rotate the flow vector to the surface tangent direction.

In internal flows, the small correction angle on the nozzle wall has an opposite sign from that of external flows in Ref. 11. Instead of applying a constant entropy condition to evaluate the gas density at the boundary, in this study the finite boundary entropy change obtained from that of the adjacent field points is utilized for the evaluation of gas density at the boundary. The similar concept of using the adjacent field point to approximate the wall entropy change in a shock-capturing approach was introduced in Ref. 12 for single-phase flows and extended to multiphase flows in Ref. 13. The three velocity components of the gas phase are computed from a surface tangency condition similar to that given in Refs. 6 and 11. For solid phase, the particle temperature and density are decoded from the conservative variables, which are evaluated from a one-sided difference[11] scheme, and the surface tangency condition is again applied to three particle velocity components. In reality, particles would either "stick" to or "reflect" from the wall[14] in a complicated manner, which accounts for nozzle wall erosion and is still not well understood.

An idealized situation where the normal component of the particle velocity is zero has been utilized in this study. A similar calculational procedure which evaluated the flow variables at singular centerline from an averaging process shown in Ref. 6 is applied to this two-phase study.

IV. COMPARISON WITH SPP RESULTS--AXISYMMETRIC NOZZLE

To demonstrate the advantage of the finite difference approach to two-phase supersonic nozzle flows and to establish the credibility of the CY3D2P (three- dimensional two-phase flows in cylindrical coordinates) code, developed under this study, the results of the calculation for an axisymmetric IUS nozzle are compared with those of the well-known SPP program.[4] Figure 2 shows the nozzle and exit cone geometry for an IUS small motor. The gas and particle properties are the same as those given in Ref. 3 as follows:

$$\bar{C}_p = 1.88 \text{ KJ/kg-K} \ (0.45 \text{ Btu/lb}_m\text{-}^oR)$$

$$\bar{C}_j = 1.34 \text{ KJ/kg-K} \ (0.32 \text{ Btu/lb}_m\text{-}^oR)$$

$$\bar{\mu}_{tl} = 8.444 \times 10^{-5} \text{Pa.s} \ (5.67 \times 10^{-5} \text{lb}_m/\text{ft-s})$$

$$\bar{m}_j = 3203.69 \text{ kg/m}^3 \ (200 \text{ lb}_m/\text{ft}^3)$$

$$Pr = 0.269 \qquad \emptyset = 30\% \qquad A = 0.65$$

$$\bar{r}_j = 2.5\mu \qquad \gamma = 1.19$$

The flow variables at $Z/r_t = 2.32$ obtained from the SPP code (1981) and shown in Fig. 3 are utilized as initial data for CY3D2P calculation. Figure 4 compares the results from the two programs at $Z/r_t = 10$. The same number of initial data points ($= 30$) is used for both calculations. In general, fairly good agreement between the results of the present finite difference approach and those of the updated 1981 SPP code is obtained. The SPP code of the 1975 version contained inadequate centerline calculation procedures and would result in erroneous flow variables at the singular centerline. For detailed flowfield comparison, the updated 1981 SPP code should be used.
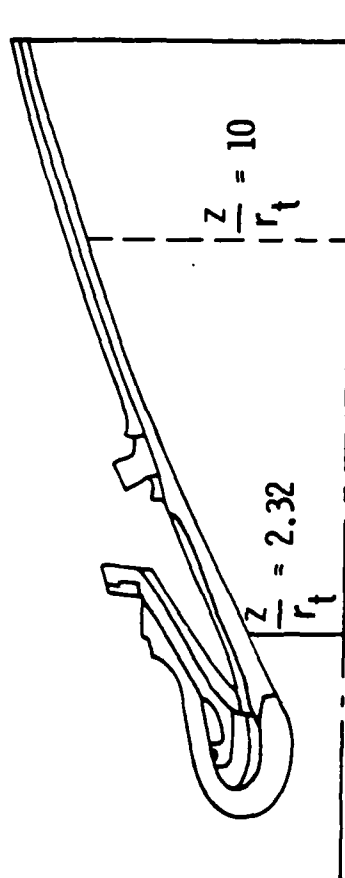
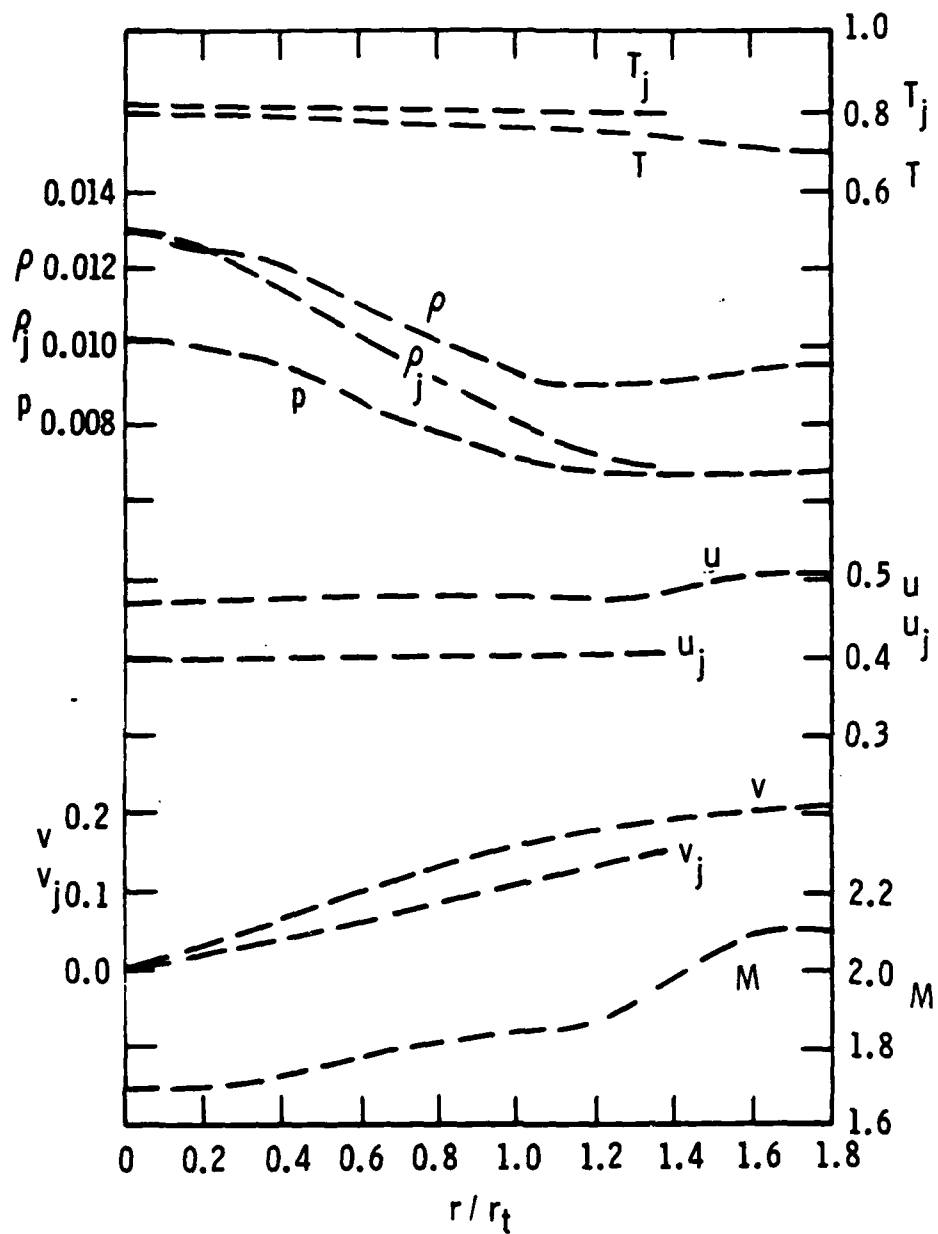Fig. 2. IUS Small Motor Exit Cone Configuration

Fig. 3. Flow Variables at $z/r_1 = 2.32$ from SPP Code
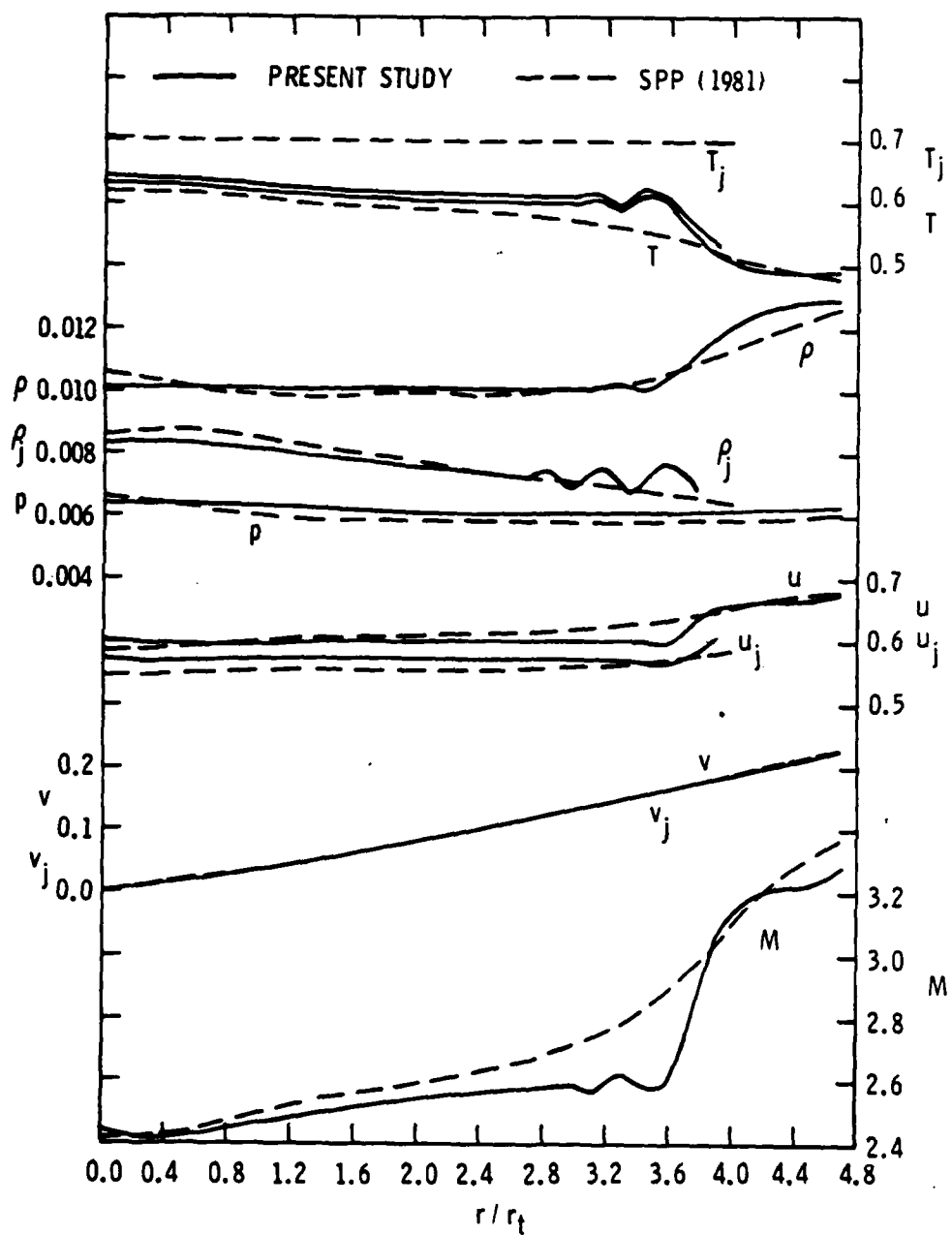(IUS small motor exit cone)

19

Fig. 4. Comparison of Flow Variables from SPP and Present
         Study at z/r_1 = 10 (IUS small motor exit cone)

20

For the nozzle geometry and gas-particle properties considered, the particle phase in the SPP code is still undergoing a liquid-to-solid phase change state and maintains at a constant particle solidification temperature. No provision has been made in the CY3D2P program for particle phase change, and a lower particle temperature associated with flow expansion in the exit cone is observed in the finite difference approach than that of SPP code. Since different particle drag coefficient formulas are used in the two methods, no such good agreement between the results from the method of characteristics and those from the present finite difference technique in the two-phase flow calculations is expected as that in the one-phase flow given in Ref. 6. Moreover, the present results show some "wiggles" near the region of particle free zone at $Z/r_1 = 10$, which is a consequence of adopting abrupt change of particle flow variables for the distinct limiting particle streamline at the initial data plane. The axial flow Mach numbers for different particle sizes, illustrated in Fig. 5, show that increasing particle size does not necessarily result in two-phase flow approaching one-phase flow solution in a supersonic nozzle. An obvious way to make a two-phase flow approach one-phase flow inside the entire supersonic nozzle is through a reduction in particle mass fraction.
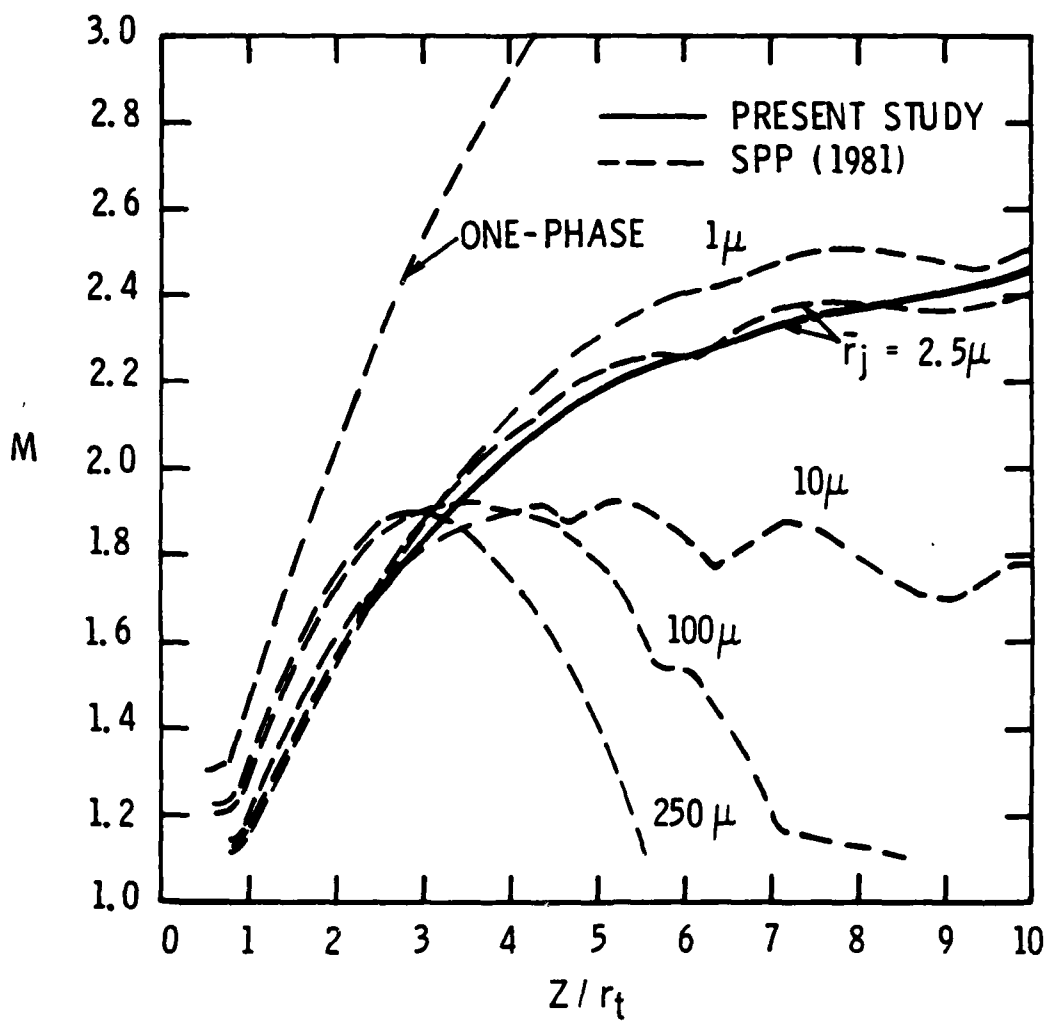
Fig. 5. Axial Flow Mach Numbers for Different Particle Sizes
(IUS small motor exit cone)

V. NUMERICAL RESULTS--THREE-DIMENSIONAL NOZZLES

The nozzle cross section considered in this study is given by the superelliptic equation[6]

$$r_W = \left[\left(\frac{\sin\theta}{r_a} \right)^n + \left(\frac{\cos\theta}{r_b} \right)^n \right]^{-1/n} \quad \text{for } n \geq 2 \tag{11}$$

The variation of the geometric parameters along the longitudinal z direction is described by a cosine curve of expansion and compression profile of the following form:

$$h = \frac{h_e + h_i}{2} + \frac{h_e - h_i}{2} \cos\left(\frac{z_s - z}{z_s} \pi \right) \quad \text{for } z_i \leq z \leq z_s$$

$$= h_e \quad \text{for } z \geq z_s \tag{12}$$

where h stands for r_a, r_b, or n, and z_s stands for some location between the initial z_i and the end z_e station along the longitudinal z direction. In this study, $z_i = 0.0$ and $z_s = 5.0$. The reference scale $\bar{L}$ in the two-phase flow calculation has been set equal to unit foot, and the initial cross section at z = 0.0 is a circular profile with $r_a = r_b = 1$ and n = 2. The flow at the inlet plane is a uniform Mach 3.

Figure 6 illustrates the cross-sectional grids (21 x 19, 21 points in r direction and 19 in θ direction) at different z stations for a rounded square nozzle with a 90° cross-sectional flow region. The superelliptic parameters vary from the initial values to $r_a = r_b = 1.5$ and n = 5 at $z_s = 5.0$, according to Eq. (12). Figure 7 shows the computed three-dimensional Mach number contours for a clean gas flow (γ = 1.4), where the index N is set to 1 in Eq. (1).
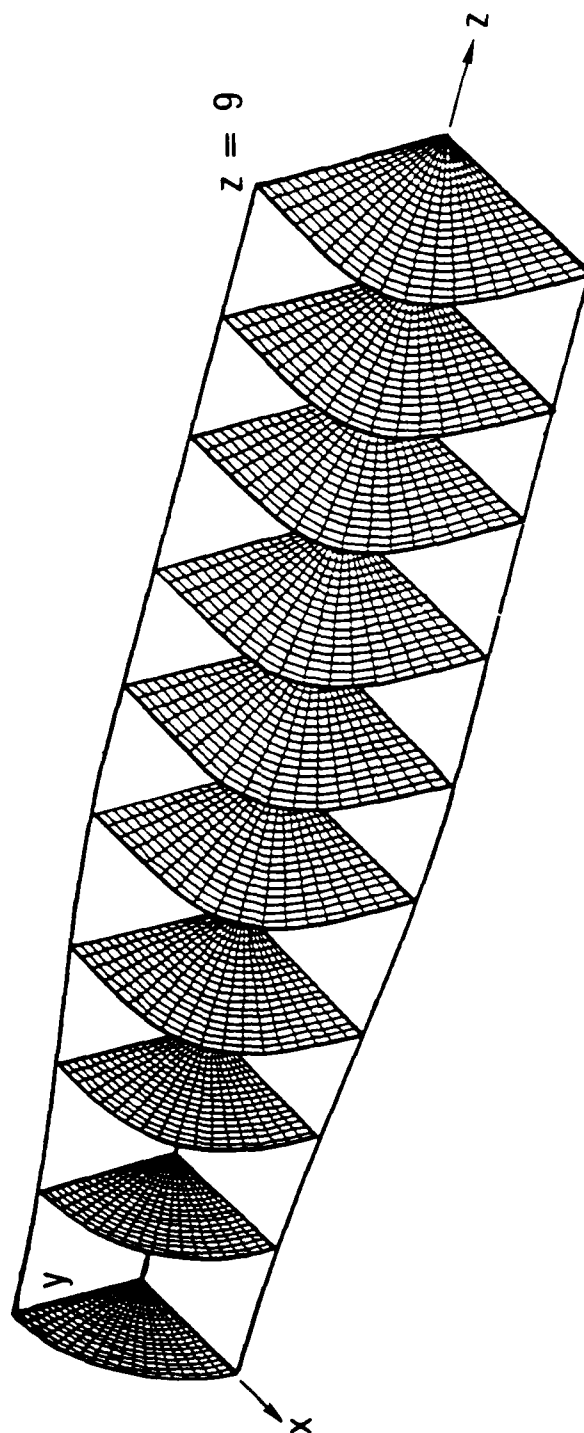
Fig. 6. Cross-Sectional Grids for Rounded Square Nozzle

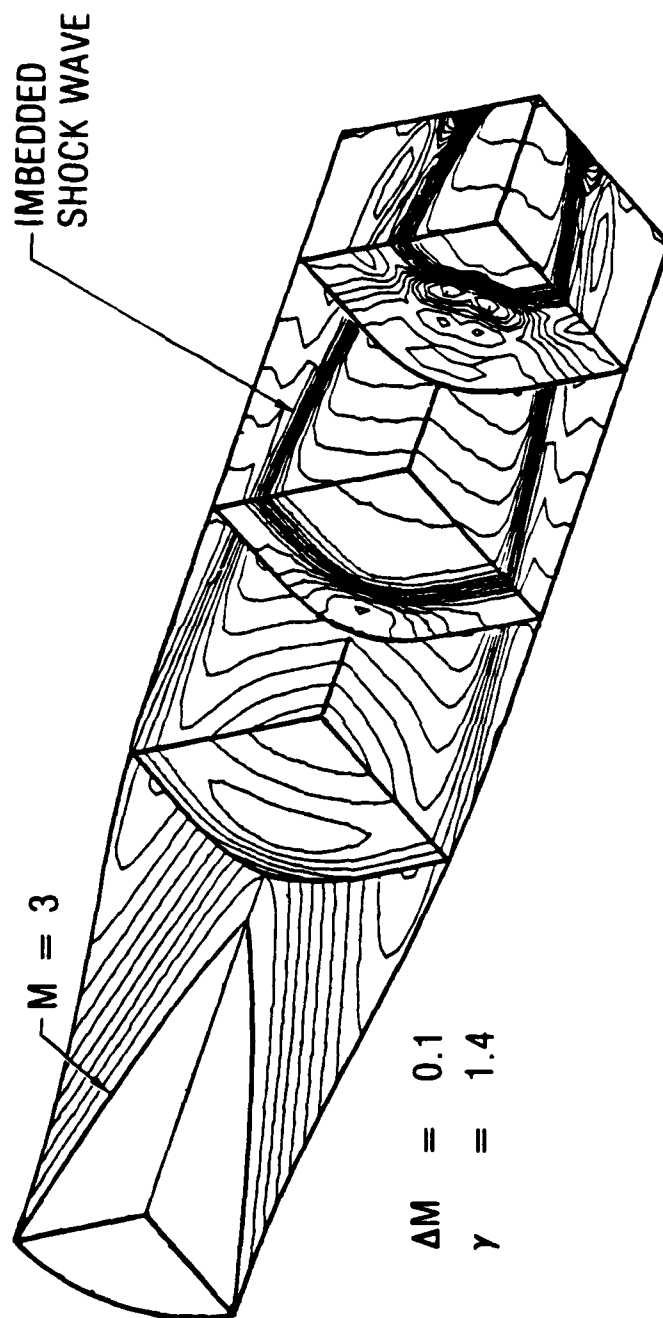IMBEDDED
SHOCK WAVE

M = 3

ΔM = 0.1
γ = 1.4

Fig. 7. Mach Number Contour for Rounded Square Nozzle (one-phase flow)

For two-phase calculation, the gas and particle data are taken to be the same as those used in Ref. 3.

<div align="center">

Gas Phase   Particle Phase

</div>

$\bar{C}_p$ = 2.68 KJ/kg-K (0.64 Btu/lb$_m$-^{o}R) $\bar{C}_j$ = 1.38 kJ/kg-K (0.33 Btu/lb$_m$-^{o}R)

$\bar{\mu}_{t1}$ = 8.88x10^{-5}Pa.s (5.97x10^{-5}lb$_m$/ft-s) $\bar{m}_j$ = 3203.69 kg/m^3 (200 lb$_m$/ft^3)

Pr = 0.45 $\emptyset$ = 28.8%

A = 0.664

The two-phase index N is set to 2, and unit velocity lag and temperature ratio, $\lambda_q = \lambda_T = 1$, is assumed at the inlet plane, z = 0. The computed Mach number contours for a two-phase flow (γ = 1.4, $\bar{r}_j$ = 6 μ) are given in Fig. 8.

Figure 9 compares the boundary Mach number distribution for various one- and two-phase flows along the meridional direction at z = 2, 4, 6, and 8, and Fig. 10 presents the similar results along one of the symmetry boundary planes. Because of flow symmetry with respect to a θ = 45° plane for the rounded square nozzle, only a 45° region is plotted in Fig. 9. At the same gas specific heat ratio, the one-phase flow has higher Mach numbers on the boundary than that of the two-phase flow, except near the region downstream of the shock as evidenced at z = 8 in Fig. 10, since the imbedded shock strength is stronger for the clean gas flow than for the flow with particles. The wave structure in the two-phase flow is different from that of the one-phase flow. For both the one- and the two-phase flow with the same particle size, lower gas specific heat ratio results in lower Mach numbers. Since hot combustion product from a solid rocket chamber usually contains gaseous phase with lower specific heat ratio than that of the gas in the cold flow test facility, the data obtained from the cold flow test should be used with discretion when utilized for the flight design consideration. Moreover, at the same gas specific heat ratio and particle mass fraction, the gas phase in large particle two-phase supersonic flow is more susceptible to the nozzle boundary geometry change than that in small particle flow, implying that the small-sized particle
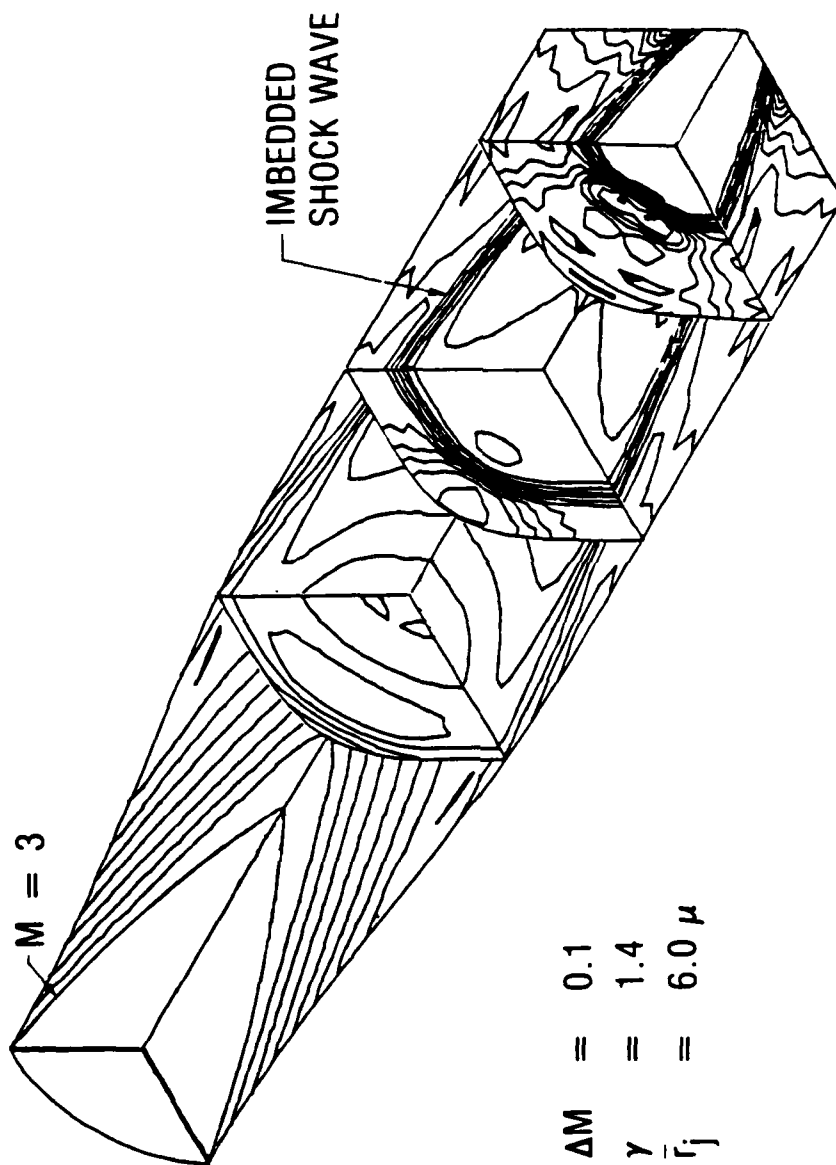
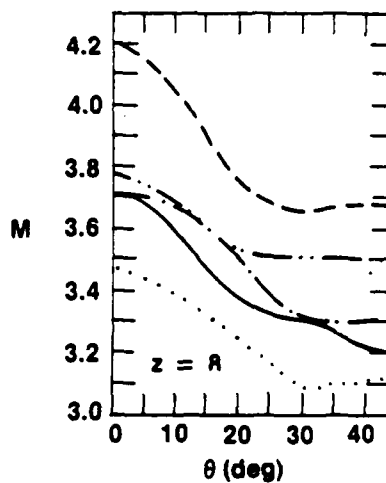Fig. 8. Mach Number Contour for Rounded Square Nozzle (two-phase flow)
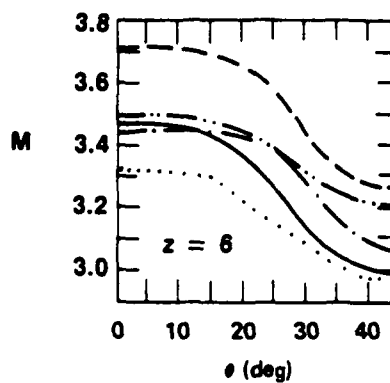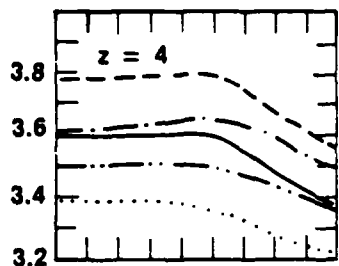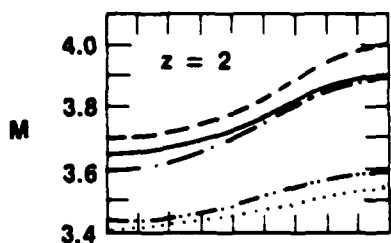
$\Delta M = 0.1$

$\gamma = 1.4$

$\bar{r}_j = 6.0 \, \mu$

M = 3

IMBEDDED SHOCK WAVE

Fig. 9. Boundary Mach Number Distribution Along Meridional Direction
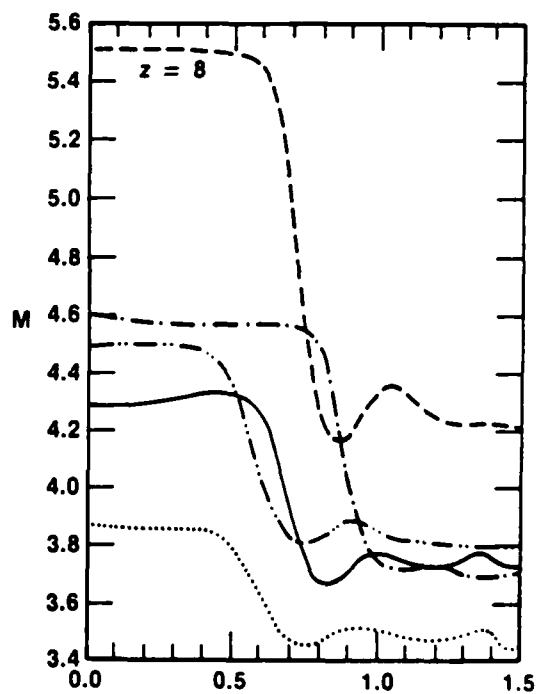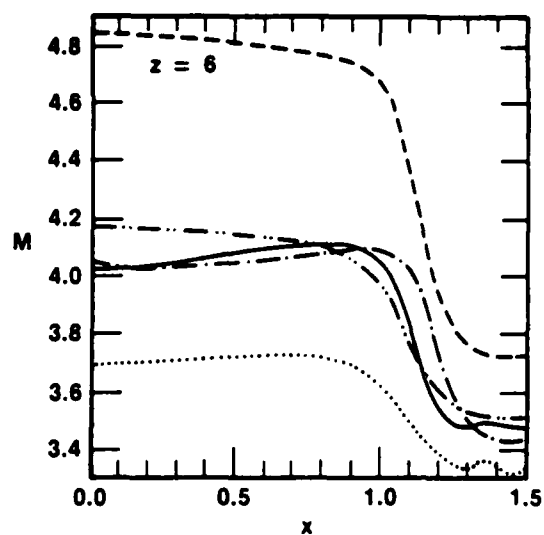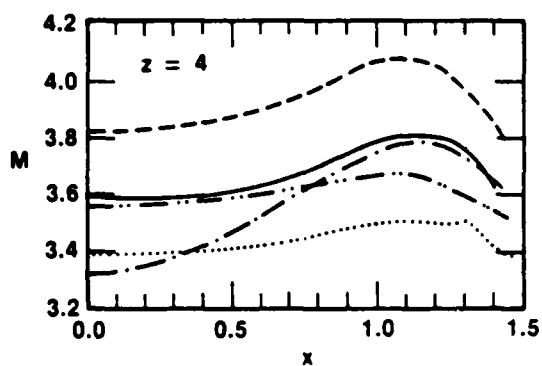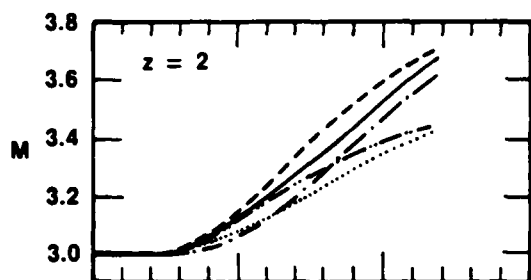for Rounded Square Nozzles

Fig. 10.   Boundary Mach Number Distribution Along x Direction
for Rounded Square Nozzle

acts more effectively to retard both gas-phase expansion and compression than that of large-sized particles. Figure 11 is the computed three-dimensional particle density contour at $\gamma = 1.4$, $\bar{r}_j = 6$ μ. A clear particle-free zone is observed from the calculated results. The particle impinges on the boundary at $z \approx 6.5$, indicating a region of high heating and erosion inside the nozzle. The information is useful to nozzle insulation study.

Whether a relaxation zone[14] appears behind the imbedded shock wave in a nonuniform multidimensional two-phase nozzle flowfield depends upon the flow condition in front of the shock wave and upon the particle size. The relaxation zone is regarded to be the transition region where particle velocity immediately behind the shock is higher than gas velocity, and particle phase reaches equilibrium state with gas phase further downstream of the shock. Figure 12 shows the gas and particle velocity distribution along one of the symmetry boundary planes at $z = 6$ and $z = 8$ for the flow with $\gamma = 1.4$, $\bar{r}_j = 1\mu$. For this small particle two-phase flow, the particle velocity downstream of the shock is higher than gas velocity and a relaxation zone ensues, similar to that discussed in Refs. 14 and 15. However, for a large particle flow, different shocked flow behavior is observed. Figure 13 shows the gas and particle velocity distribution for the flow with $\bar{r}_j = 6$ μ at the same locations. No relaxation zone is possible for this large particle flow, since both the particle velocities in front of and behind the imbedded shock wave are lower than the corresponding gas velocities and an equilibrium state for gas and particle does not exist. Obviously, the results shown in Figs. 12 and 13 are the direct consequence of assumed particle drag coefficient and heat transfer formulation. Different formulations would affect the computed flowfield. The discussions given in Refs. 14 and 15 on the existence of a relaxation zone behind a shock wave in a two-phase flow are, strictly speaking, applicable only for a homogeneous uniform one-dimensional two-phase mixture in front of the shock wave.

PARTICLE IMPINGEMENT REGION

PARTICLE FREE ZONE

$\rho_j = 0.03$

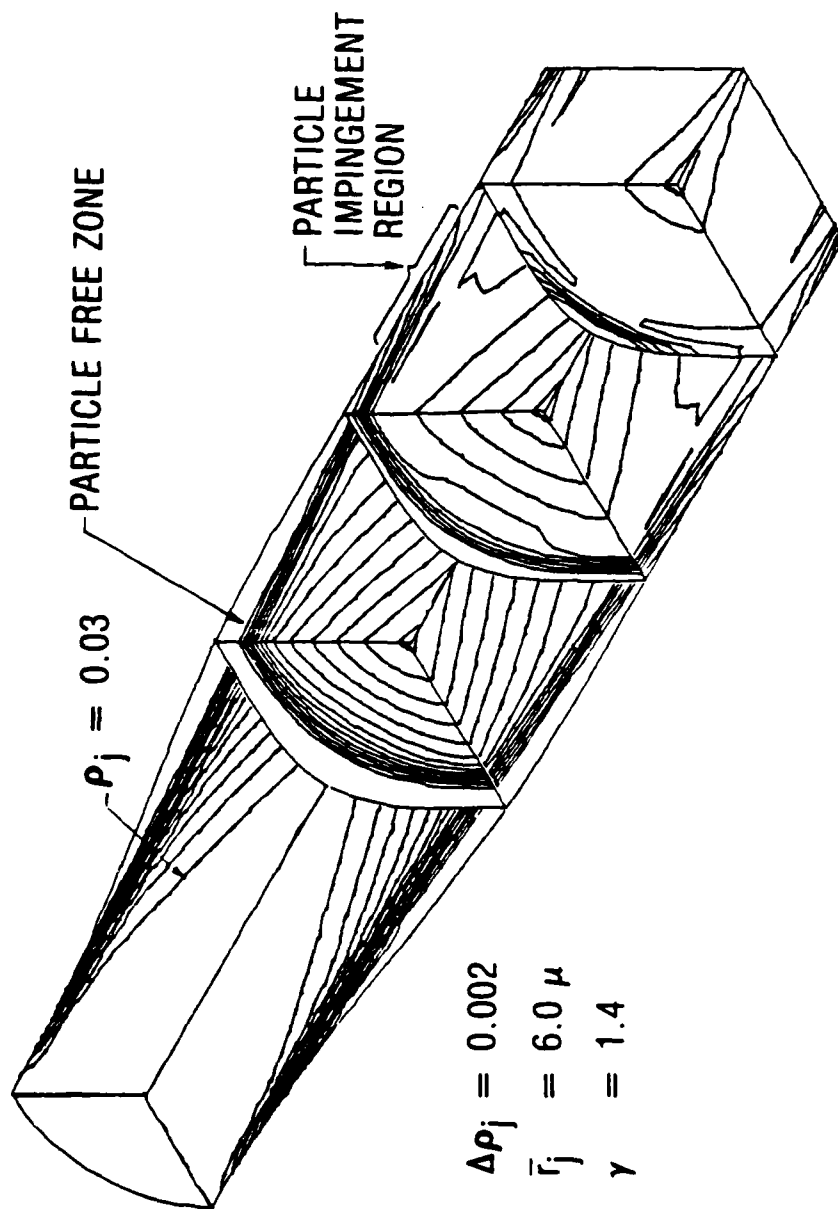$\Delta \rho_j = 0.002$

$\bar{r}_j = 6.0 \mu$

$\gamma = 1.4$

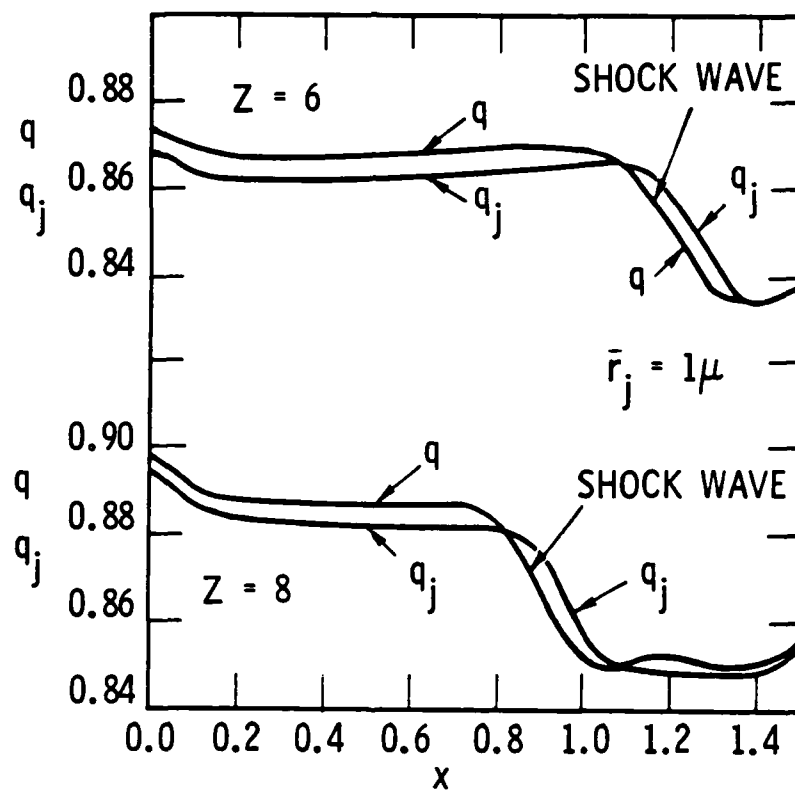Fig. 11. Particle Density Contour for Rounded Square Nozzle

Fig. 12.   Gas and Particle Velocity for $\bar{r}_j = 1\mu$--with
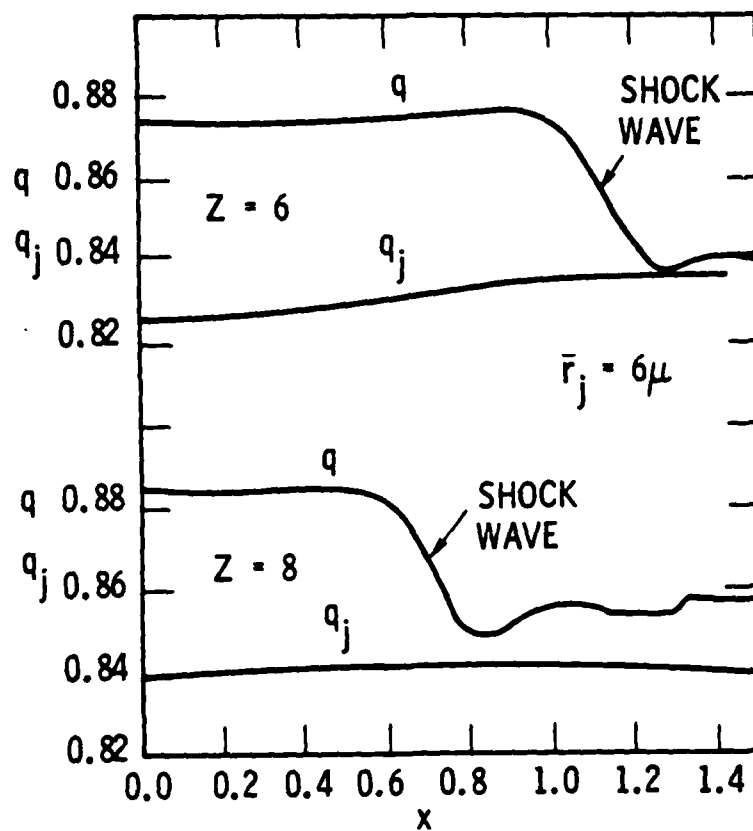Relaxation Zone Behind Imbedded Shock Wave

Fig. 13. Gas and Particle Velocity for $\bar{r}_j = 6\mu$--without Relaxation Zone Behind Imbedded Shock Wave

Figure 14 illustrates computed flow Mach number at the centerline of the symmetry plane. The similar effect of particle size variation on the flow behavior as that of axisymmetric flow shown in Fig. 5 is observed for the three-dimensional flow inside the rounded square nozzle. The computer program with the array dimensioned for a 31 x 37 cross-sectional grid occupies 151,000 (octal) small core and 214,000 (octal) large core on a CDC Cyber 176 computer, and a typical run for the two-phase flow inside the rounded square nozzle with 21 x 19 cross-sectional grid takes 2 min, 10 sec.

The cross-sectional grids at different z stations inside an elliptic nozzle with 90° cross-sectional flow region are illustrated in Fig. 15. The geometric parameters vary smoothly from the initial values to $r_a = 1.0$, $r_b = 1.5$, and n = 2 at z = 5.0. The same inflow condition as the rounded square nozzle is used for the elliptic nozzle calculation. Figure 16 depicts the computed particle density contour, which shows that a smaller particle-free zone existed in the elliptic nozzle than that in the rounded square nozzle. Figures 17 and 18 compare the difference in Mach number contours in the elliptic nozzle for one- and two-phase supersonic flows. The compression waves generated from the boundary coalesce into a weak shock wave, which impinges on the centerline of the elliptic nozzle earlier than that of the rounded square nozzle in both one- and two-phase flows. The comments made in Ref. 6 regarding the dependence of the flowfield on the nozzle geometric configuration for the clean gas flow are equally applicable to the two-phase flow.

Finally, a hybrid nozzle, which is composed of half circular ($0 \leq \theta \leq 90°$) and half rounded-square ($90° \leq \theta \leq 180°$) regions is depicted in Fig. 19 to illustrate the calculation with a 180° cross-sectional flow region (21 x 25). The superelliptic parameters vary from the initial values to $r_a = r_b = 1.5$ and n = 2 for the circular portion and to $r_a = r_b = 1.5$ and n = 5 for the rounded-square portion of the nozzle at z = 5.0. Figure 20 shows the computed particle density contours for the two-phase flow with $r_j = 6\mu$ and $\gamma = 1.19$. Because of a smaller gas specific heat ratio, the value of the nondimensionalized particle density given in Fig. 20 is smaller than that in Fig. 11. A
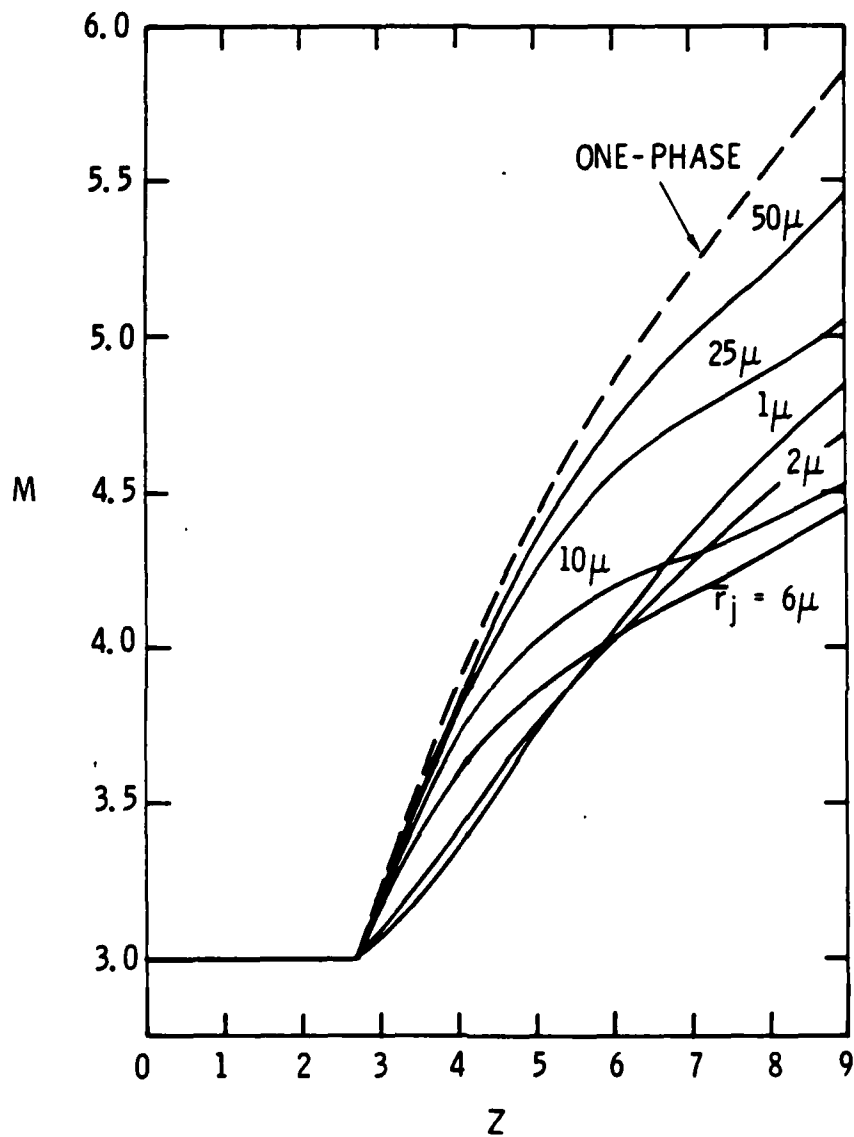
Fig. 14.   Flow Mach Numbers at the Centerline of Symmetry Plane
for Different Particle Sizes (rounded square nozzle)
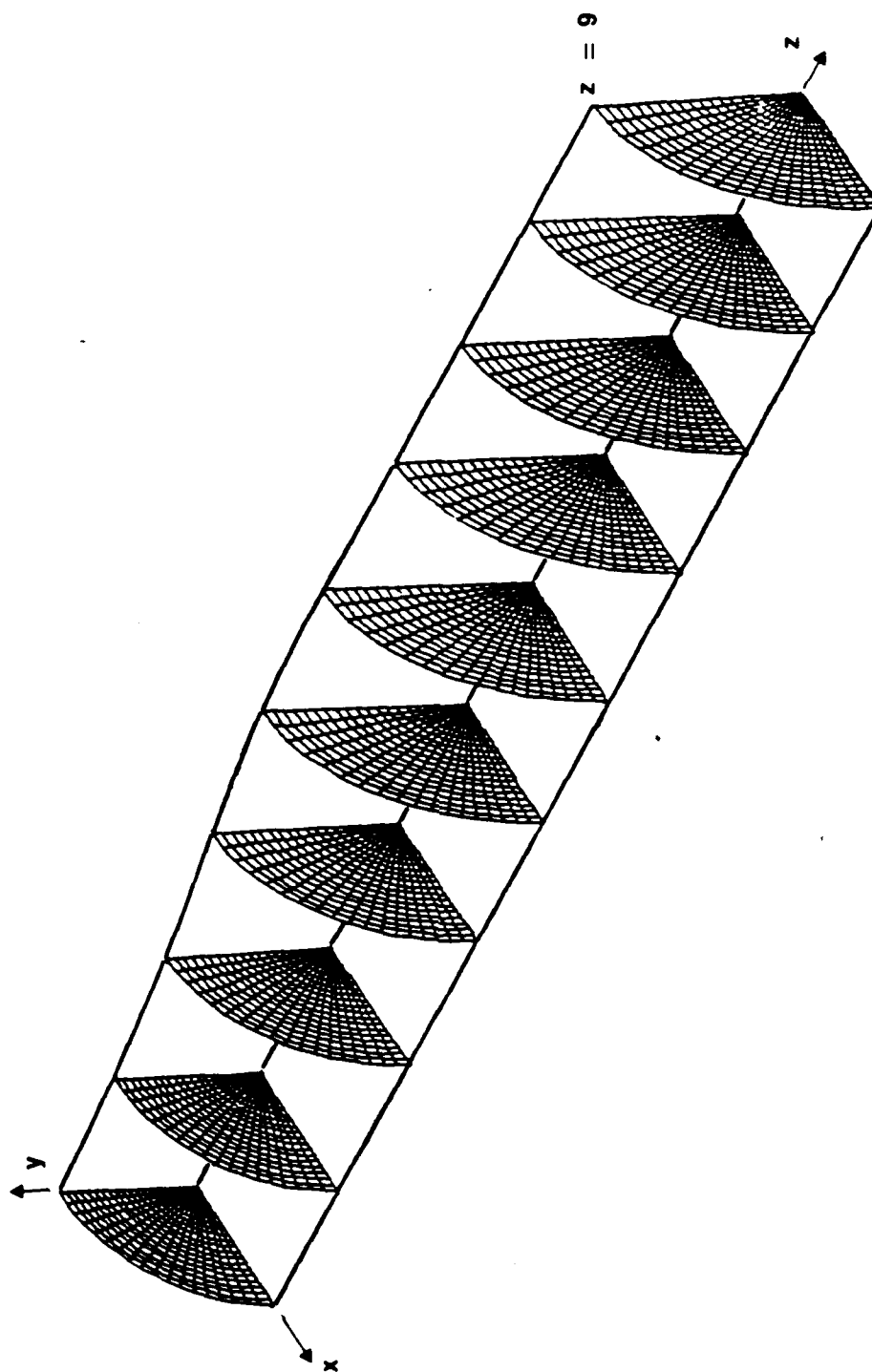
Fig. 15. Cross-Sectional Grids for Elliptic Nozzle

$\rho_j = 0.03$

$\Delta\rho_j = 0.002$

$\gamma = 1.4$

$\frac{r}{r_j} = 6.0\,\mu$
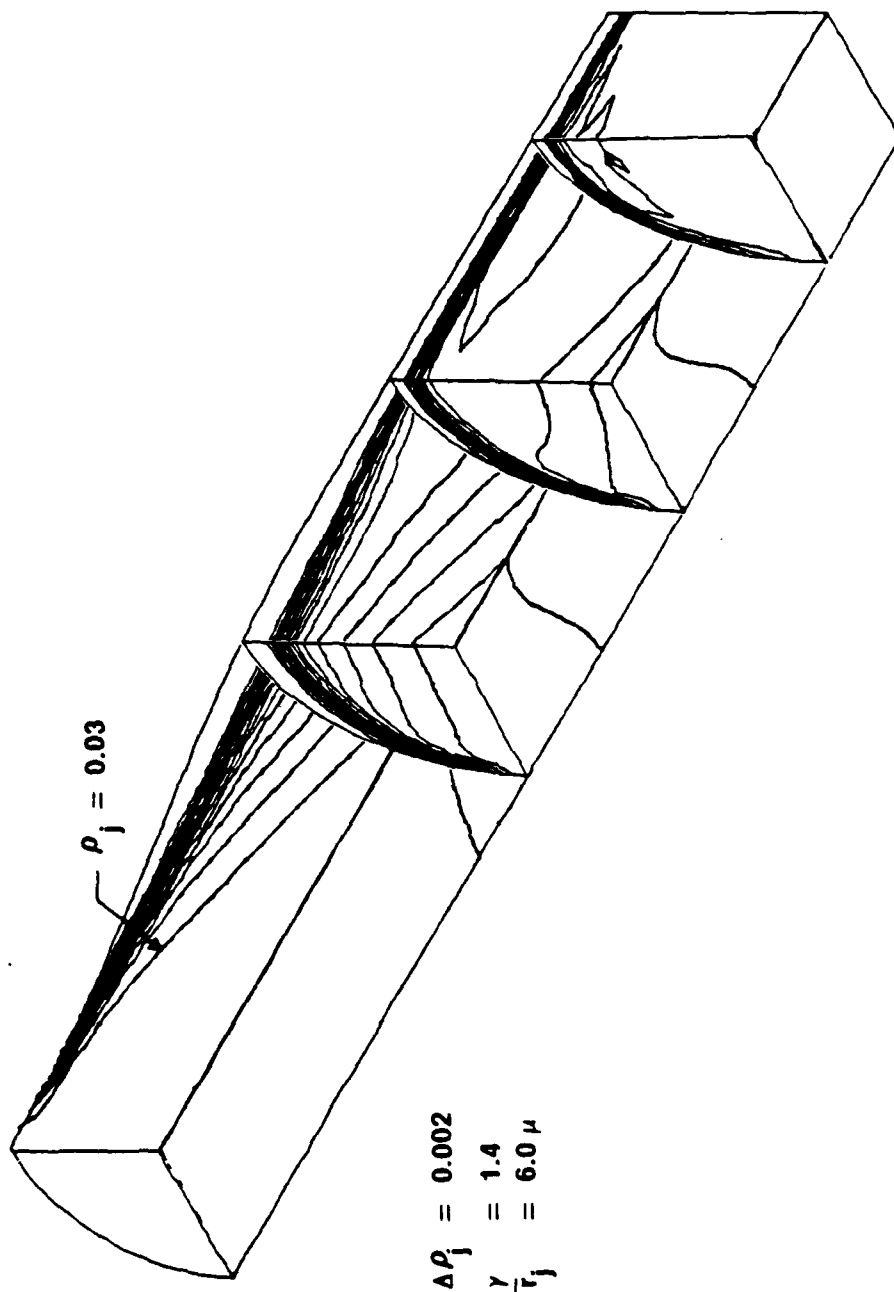
Fig. 16. Particle Density Contour for Elliptic Nozzle

37

M = 3

$\Delta M = 0.1$
$\gamma = 1.4$
$\dfrac{r}{r_j} = 6.0\,\mu$
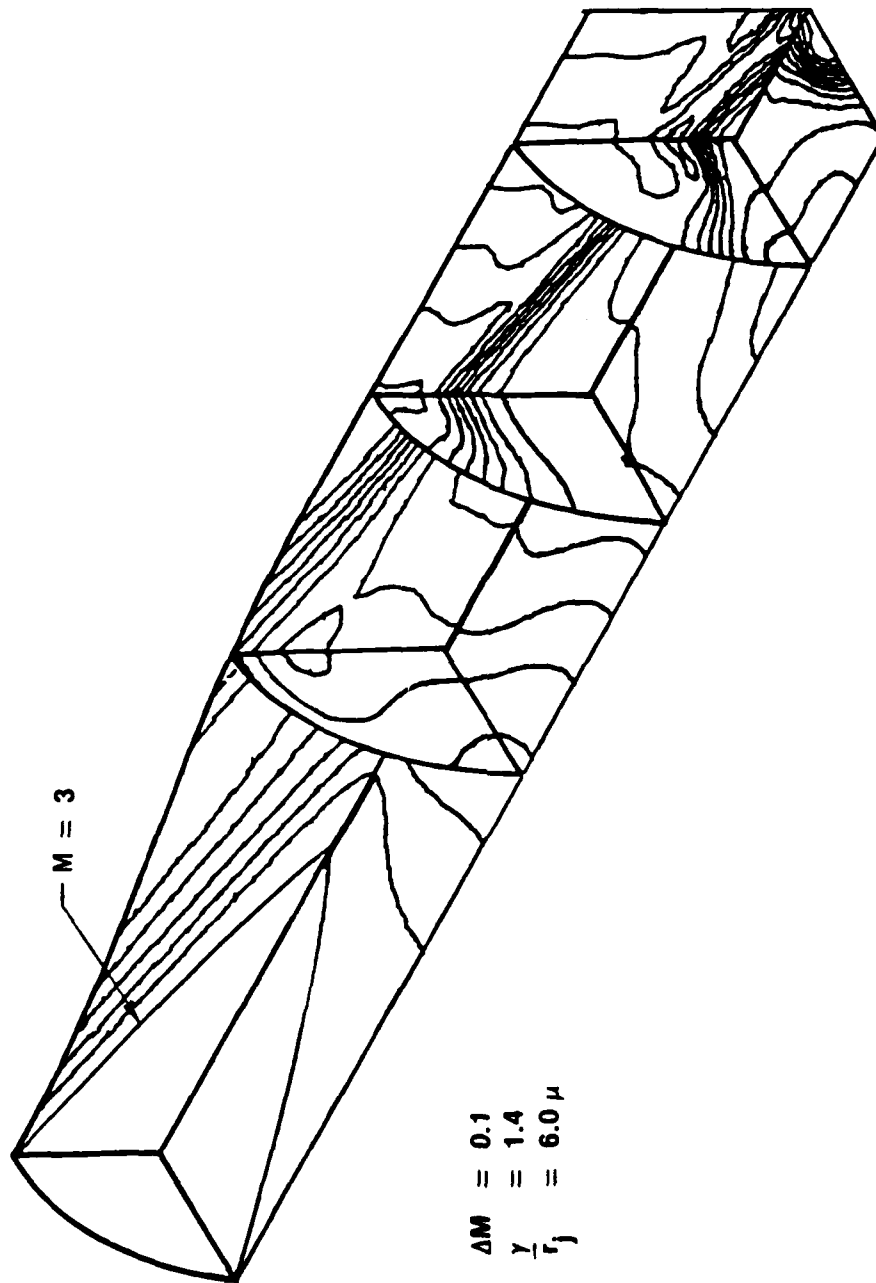
Fig. 17. Mach Number Contour for Elliptic Nozzle
(two-phase flow)

38

M = 3

$\Delta M = 0.1$
$\gamma = 1.4$
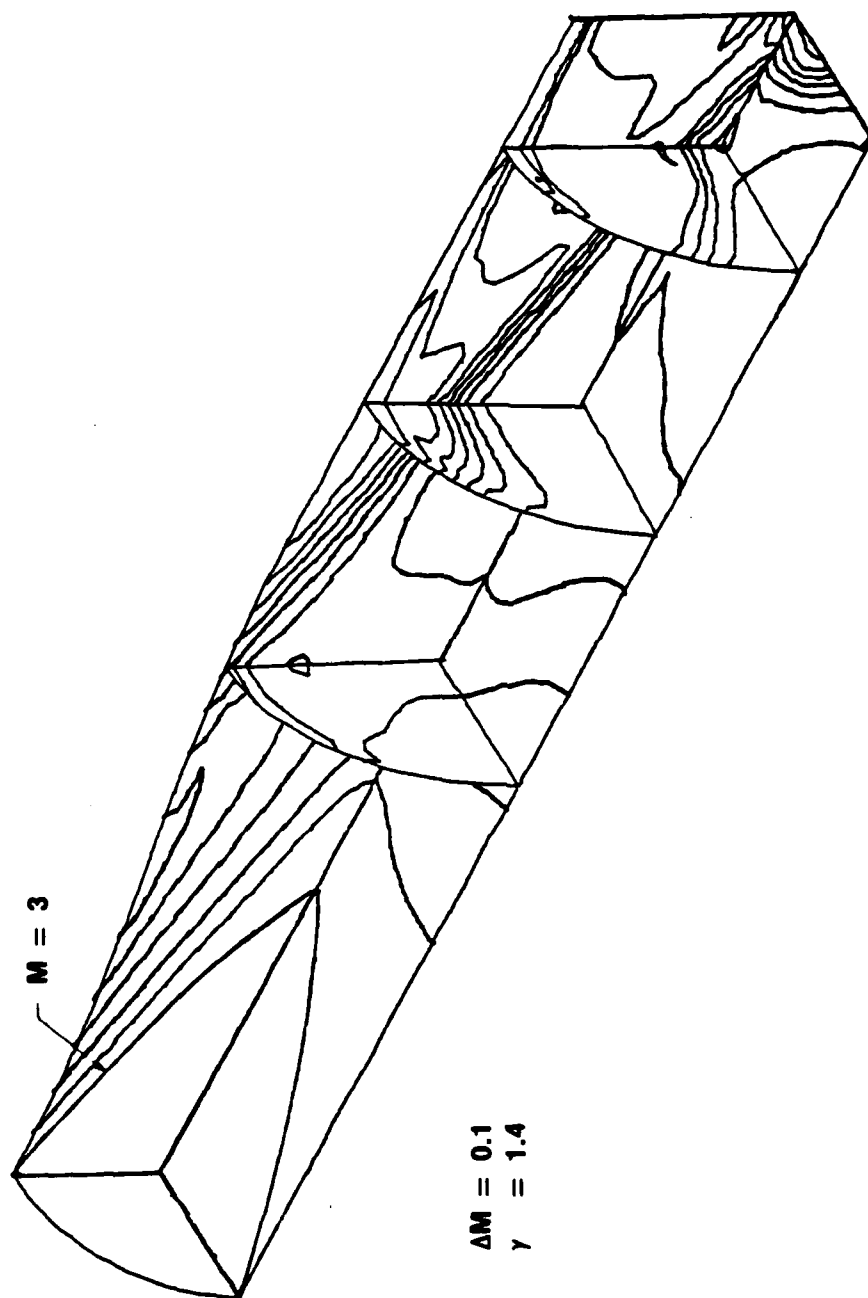
Fig. 18. Mach Number Contour for Elliptic Nozzle
(one-phase flow)
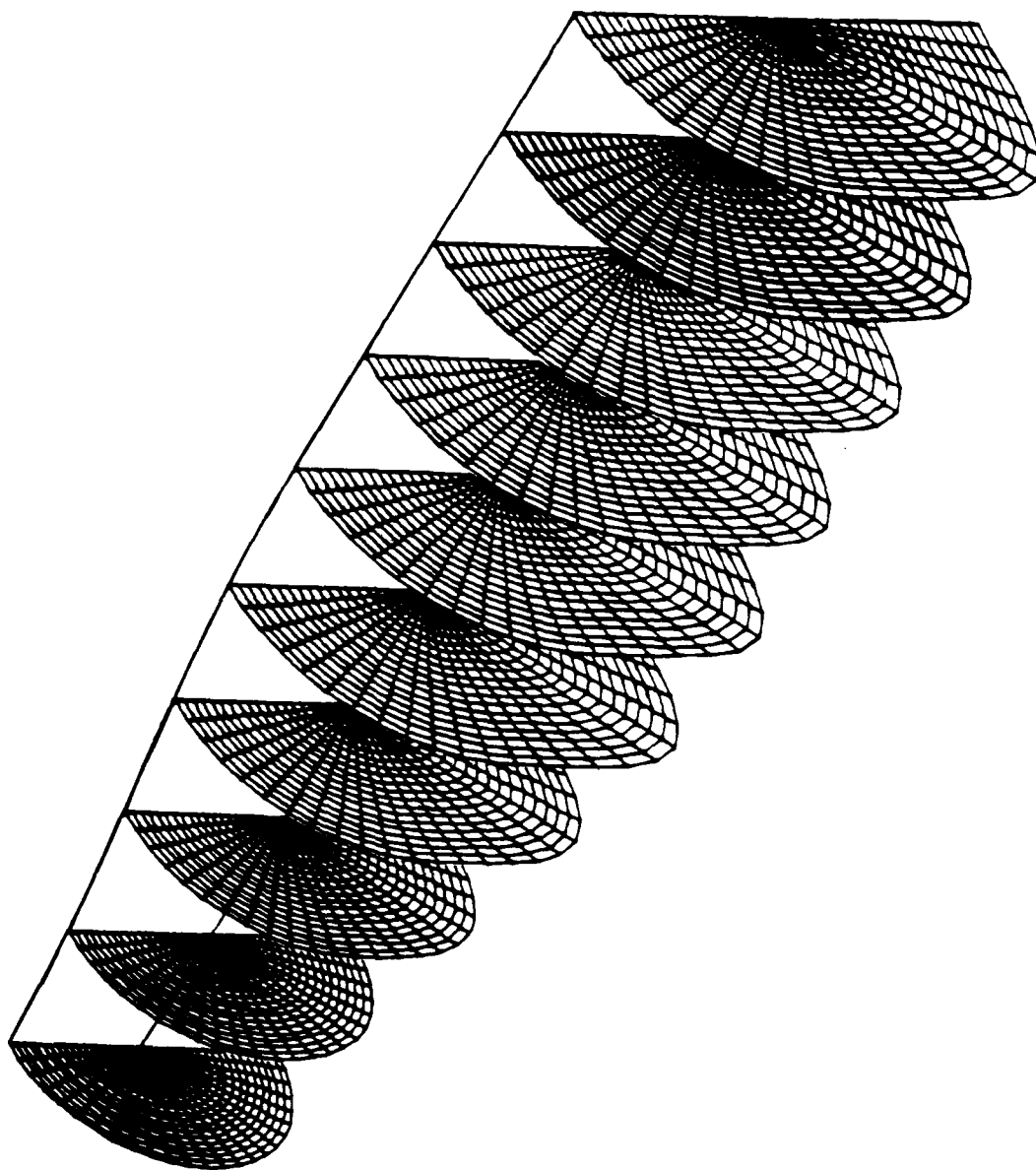
Fig. 19. Cross-Sectional Grids for Hybrid Nozzle

PARTICLE IMPINGEMENT REGION

PARTICLE FREE ZONE

PARTICLE FREE ZONE

$\rho_j = 0.015$

$\Delta\rho_j = 0.001$

$\bar{r}_j = 6.0\,\mu$

$\gamma = 1.19$
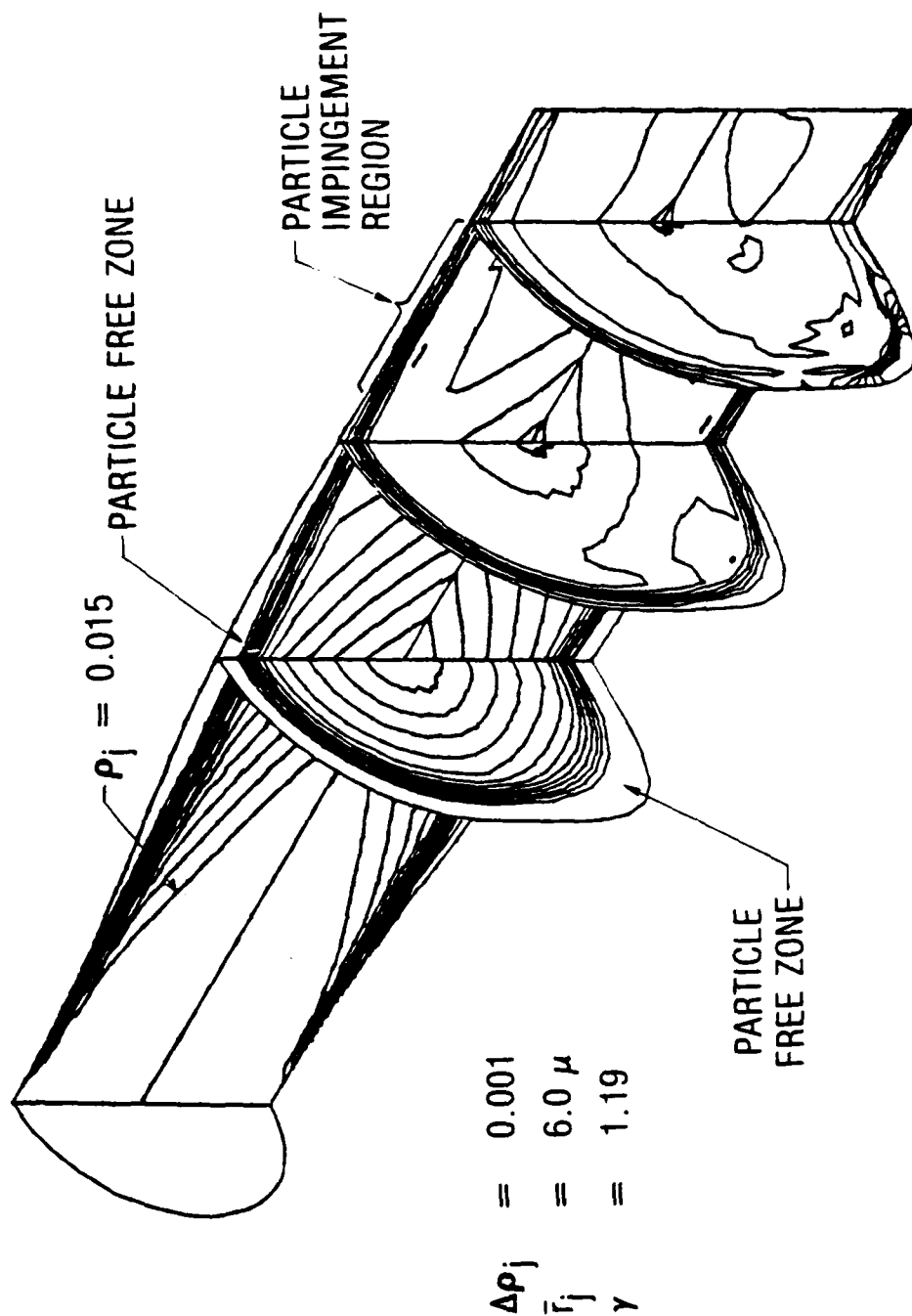
Fig. 20. Particle Density Contour for Hybrid Nozzle

41

uniform Mach 3 flow at the inlet plane means that changing γ from 1.4 to 1.19 causes the reduction of the ratio of gas static to reference stagnation density by a factor of 1.97, according to the isentropic relationship. The same factor is carried over to the dimensionless particle density value of the inlet plane, since the particle mass fraction and the reference state remain the same. Figures 21 and 22 compare the Mach number contours for the one- and two-phase flows, respectively. It is obvious from these Mach number contour curves that the introduction of $r_j = 6\mu$ particles in the gas flowfields alleviates the contour clustering and, hence, the shock strength by approximately 30 percent. This perhaps explains why the performance calculation from the method of characteristics fortuitously predicts a result which agrees relatively well with that from motor test firing, even though a shockless flowfield is tacitly assumed to prevail in Ref. 4.

IMBEDDED
SHOCK WAVE

M = 3

ΔM = 0.1
$\bar{r}_j$ = 6.0 μ
γ = 1.19
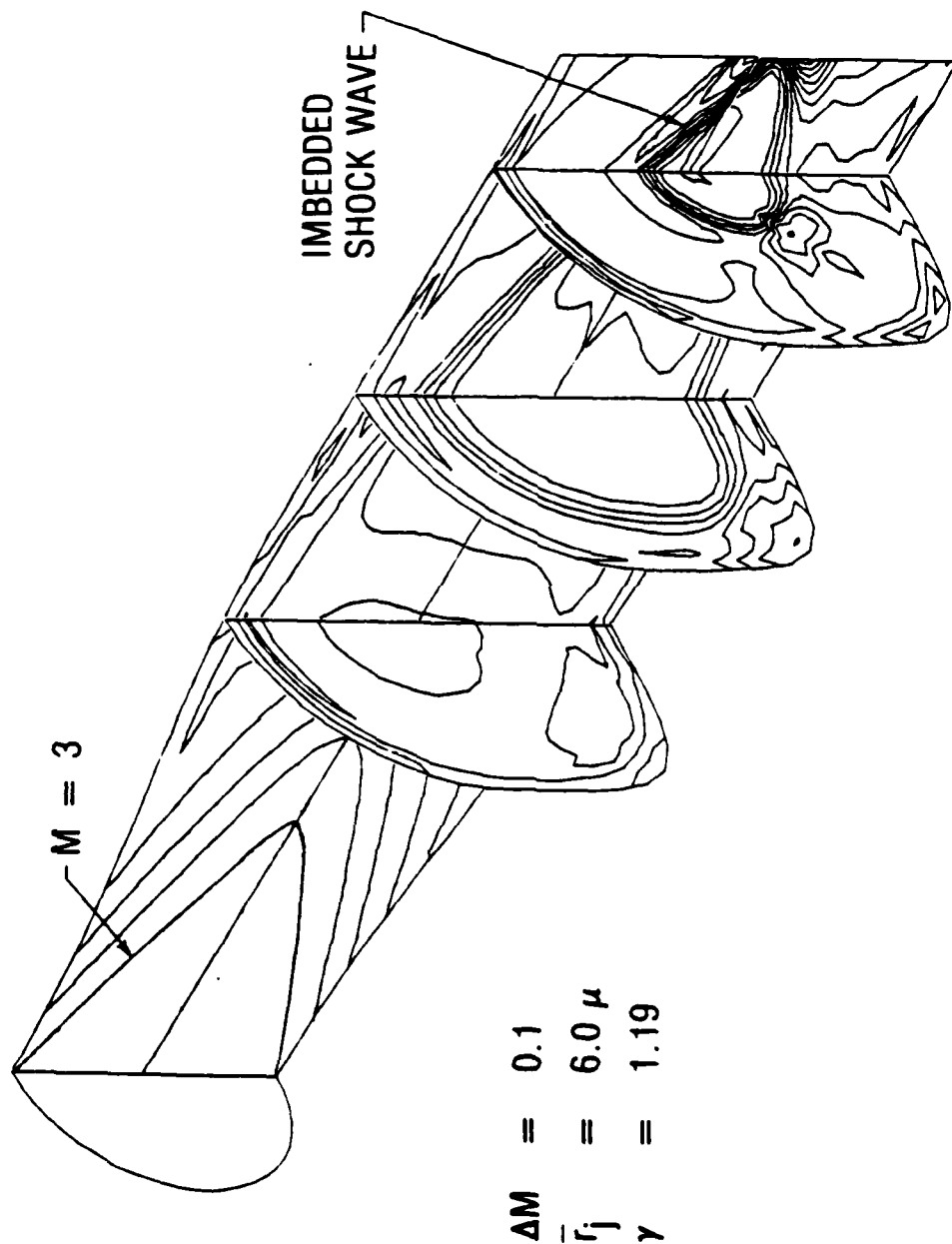
Fig. 21. Mach Number Contour for Hybrid Nozzle (two-phase flow)

IMBEDDED SHOCK WAVE

M = 3

$\Delta M \quad = \quad 0.1$

$\bar{r}_j \quad = \quad 6.0 \, \mu$

$\gamma \quad = \quad 1.19$

Fig. 22. Mach Number Contour for Hybrid Nozzle (one-phase flow)

44

VI. CONCLUSION

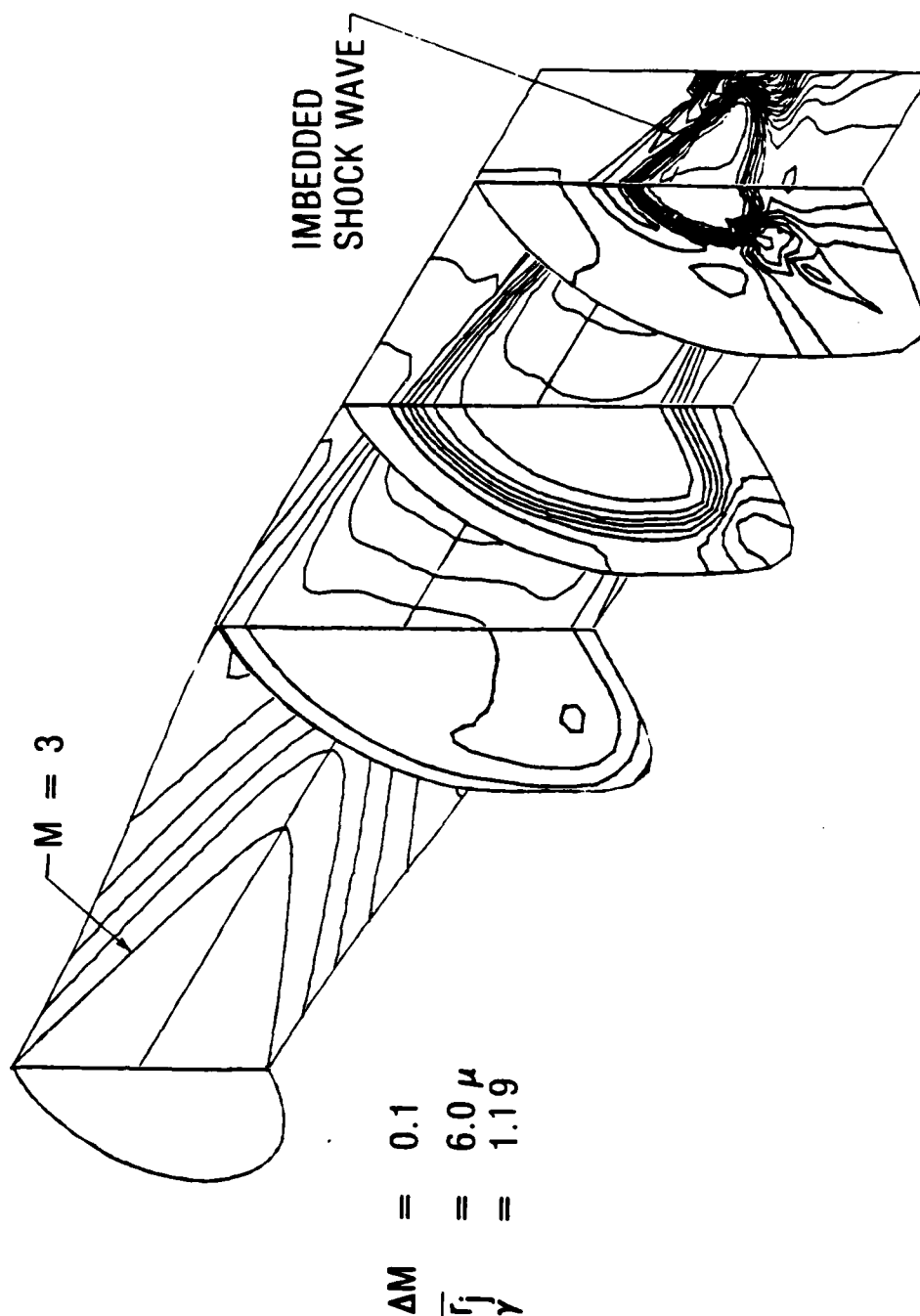Idealized two-phase supersonic flows inside an axisymmetric IUS small motor nozzle and various three-dimensional nozzles have been studied numerically. The study stressed the importance of the proper treatment of boundary flow variables for a two-phase flowfield calculation, even in the absence of a pertinent particle impingement model. Subject to the provision that the particular particle drag law for spherical particles and the simple particle convective and radiative heat transfer relationships have been adopted in the study, the computed results revealed the three-dimensional two-phase supersonic nozzle flow structures, which differed noticeably from those of the clean gas flows. The study also emphasized the existence and complexity of the imbedded shock inside the three-dimensional supersonic nozzles. Due to the restriction of practical nozzle physical dimensions, the complex imbedded shock structure, often ignored or assumed nonexistent in the calculation with some simplified analysis, is almost ubiquitous in a three-dimensional supersonic nozzle and can be computed with the present technique. Obviously, a three-dimensional one- or two-phase supersonic nozzle flow generally would have nonuniform flow at the inlet plane, and the starting data should be obtained from a three-dimensional subsonic-transonic flow solution, which is the subject of follow-on studies.

REFERENCES

1. Kliegel, J.R., "Gas Particle Nozzle Flows," Ninth (International) Symposium on Combustion, Academic Press, New York, 1963, p. 811.

2. Kliegel, J.R. and G.R. Nickerson, "Axisymmetric Two-Phase Perfect Gas Performance Program," TRW Systems Group, Redondo Beach, Calif., Report 02874-6006-R000, Vols. I and II, April 1967.

3. Chang, I-Shih, "One- and Two-Phase Nozzle Flows," AIAA Paper 80-0272, Jan. 1980; also, AIAA J. 18(12), Dec. 1980, p. 1455.

4. Coats, D.E., et al., "A Computer Program for the Prediction of Solid Propellant Rocket Motor Performance," Vols. I, II, and III, AFRPL-TR-75-36, July 1975. For updated version, see Vols. I and III, AFRPL-TR-80-34, April 1981.

5. Thorpe, R.D., S.M. Dash, and H.S. Pergament, "Inclusion of Gas/ Particle Interactions in a Shock-Capturing Model for Nozzle and Exhaust Plume Flows," AIAA Paper 79-1288, June 1979.

6. Chang, I-Shih, "Three-Dimensional Supersonic Internal Flows," AIAA Paper 76-423, July 1976.

7. Henderson, C.B., "Drag Coefficients of Spheres in Continuum and Rarefied Flows," AIAA J. 14(6), June 1976, p. 707.

8. Carlson, D.J. and R.F. Hoglund, "Particle Drag and Heat Transfer in Rocket Nozzles," AIAA J. 2(11), November 1964, p. 1980.

9. MacCormack, R.W., "The Effect of Viscosity in Hypervelocity Impact Cratering," AIAA Paper 69-354, May 1969.

10. Abbett, M. J., "Boundary Condition Calculation Procedures for Inviscid Supersonic Flow Fields," Proceedings of the AIAA Computational Fluid Dynamics Conference, Palm Springs, Calif., July 1973.

11. Kutler, P., W.A. Reinhardt, and R.F. Warming, "Numerical Computation of Multi-Shocked, Three-Dimensional Supersonic Flow Fields with Real Gas Effects," AIAA J. 11(5), May 1973, pp. 657-664.

12. Dash, S. M. and Del Guidice, P. D., "Three-Dimensional Ducted and Exhaust Plume Flow Fields," AIAA J., 16, August 1978, pp. 823-830.

13. Dash, S. M. and Thorpe, P. D., "Shock Capturing Model for One- and Two-Phase Flows," AIAA J., 19, July 1981, pp. 842-851.

14. Rudinger, G., "Relaxation in Gas-Particle Flow," Nonequilibrium Flows, 1 (1), P. P. Wegener (ed.), Marcel Dekker, New York, 1970, Chap. 3, pp. 119-161.

15. Carrier, G. F., "Shock Waves in a Dusty Gas," J. Fluid Mech., 4, 1958, p. 376.

a, a_1	constants used in Eq. (8)
A	exponent in the viscosity-temperature Eq. (7)
A_j	dimensionless friction term defined in Eq. (2)
b, b_1	constants used in Eq. (8)
B_j	dimensionless energy exchange term defined in Eq. (3)
C_D	particle drag coefficient
$\bar{C}_j$	particle heat capacity
$\bar{C}_p$	gas specific heat at constant pressure
e	dimensionless gas total energy/unit volume
$\tilde{E}, \tilde{F}, \tilde{G}, \tilde{H}$	vectors defined in Eq. (1)
E, F, G, H	vectors defined in Eq. (9)
f_j	momentum transfer parameter defined in Eq. (4)
g_c, g_r	convective and radiative parameters defined in Eq. (3)
h, h_e, h_i	parameters used in Eq. (12)
h_j	dimensionless particle total energy/unit volume
k_1	constant used in Eq. (8)
$\tilde{L}$	reference length scale, e.g., unit foot or unit meter
M	gas-phase Mach number
$\bar{m}_j$	particle mass density
n	superelliptic geometric index defined in Eq. (11)
N	index: $N = 1$, one-phase gas-only flow; $N = 2$, two-phase flow
Nu_j	particle Nusselt number
p	dimensionless pressure
Pr	gas-phase Prandtl number

q, q_j	dimensionless gas and particle speed, respectively
r	dimensionless radial coordinate
r_a, r_b	dimensionless nozzle wall radii on x,y axes, respectively, used in Eq. (11)
$\tilde{r}_j$	particle radius
r_W	dimensionless nozzle wall radial coordinate
r_t	dimensionless nozzle throat radial coordinate
Re_j	particle Reynolds number defined in Eq. (6)
T, T_j	dimensionless gas and particle temperature, respectively
u, v, w	dimensionless gas-phase velocity component along z, r, Θ directions, respectively
u_j, v_j, w_j	dimensionless particle-phase velocity component along z, r, Θ directions, respectively
$\bar{V}_{max1}$	adiabatic maximum speed evaluated at the inlet plane
x, y, z	dimensionless Cartesian coordinates shown in Fig. 1
γ	gas specific heat ratio
δ	geometric index: $\delta = 0$, rectangular coordinates; $\delta = 1$, cylindrical coordinates
ϵ_e	effective emissivity between gas and particle
ζ	transformed dimensionless coordinate in radial direction
η	normalized radial coordinate = r/r_W
Θ	meridional angle in cylindrical coordinates, see Fig. 1
λ_q	initial velocity lag, $\lambda_q = q_j/q$
λ_T	initial temperature ratio, $\lambda_T = T/T_j$
μ	micron, 10^{-6} m
$\bar{\mu}_g$	gas viscosity
$\bar{\mu}_{t1}$	gas viscosity at stagnation state

ξ transformed dimensionless coordinate in meridional angular direction

ρ, ρ_j dimensionless gas and particle density, respectively

$\bar{\sigma}$ Stefan-Boltzmann constant

τ $(\gamma-1)/(2\gamma)$

Θ particle mass fraction

ω $\bar{c}_j/\bar{c}_p$

Superscript

$(\rightarrow)$ vectored quantity

$(-)$ dimensioned quantity

Subscript

e   exit station

g   gas phase

i   initial station at inlet plane

j   particle phase

max1   maximum state evaluated at the inlet plane

t1   stagnation state evaluated at the inlet plane